Supplementary Materials for

Laser Direct Write of Heteroatom-Doped Graphene on Molecularly Controlled Polyimides for Electrochemical Biosensors with Nanomolar Sensitivity

*Ki-Ho Nam, Moataz Abdulhafez, Elisa Castagnola, Golnaz Najaf Tomaraei, Xinyan Tracy Cui, Mostafa Bedewy**

Corresponding author. E-mail: mbedewy@pitt.edu

Supplementary Figures

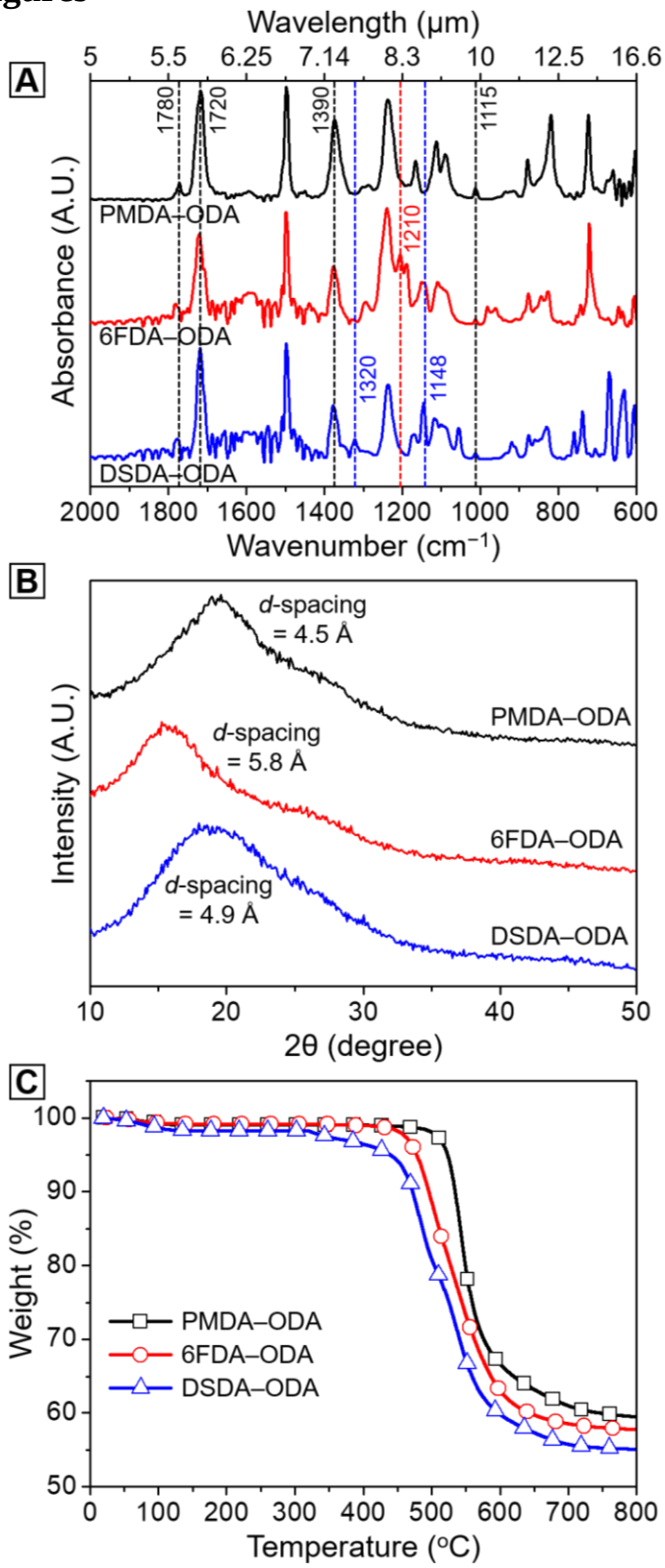

Fig. S1. (a) FTIR absorption spectra, (b) XRD patterns, and (c) TGA thermograms of PIs.

The FTIR absorption spectra of three PIs were combined in Fig. S1(a). All the PIs showed characteristic absorption peaks at 1780 cm^{-1}, 1720 cm^{-1}, and 1390 cm^{-1} corresponding to the asymmetric C=O stretching, symmetric C=O stretching, and C–N stretching, respectively.[1] No absorption peak appearing round 1650 cm^{-1} indicated that PAA was completely converted to PI during the thermal dehydration. The absorption peak at 1210 cm^{-1} was assigned to the C–F stretching in 6FDA–ODA,[2] while the absorption peaks appearing at 1320 cm^{-1} and 1148 cm^{-1} are assigned to the C–(SO_2)–C stretching and S=O stretching vibrations in DSDA–ODA.[3]

The average interchain spacing (*d*-spacing) was calculated from the most prominent XRD peak in the glassy amorphous PI spectra. From Fig. S1(b), it was observed that all the PI films presented amorphous phase. The chain packing density and intermolecular interaction of PIs with the same diamine was shown in the decreasing order of PMDA–ODA > DSDA–ODA > 6FDA–ODA. It can be explained that the 6FDA tetracarboxylic dianhydride owned bulky spatial structures, which disrupted the chain packing and reduced the polymer–polymer interaction.

The effect of molecular building blocks on the thermal degradation behavior of three PIs was evaluated using the original TGA thermograms (Fig. S1(c)). The temperatures at 5% weight loss ($T_{d5\%}$) of the PI films in nitrogen atmosphere were recorded in the range of 439–523 °C and were found to gradually increase in the order of DSDA–ODA < 6FDA–ODA < PMDA–ODA. Furthermore, carbonized residues at 800 °C were in the range of 55–59%. PMDA with relatively ordered, linear, and rigid-rod-like backbone structure showed a higher thermal stability than with the present of sulfone and bulky trifluoromethyl groups.

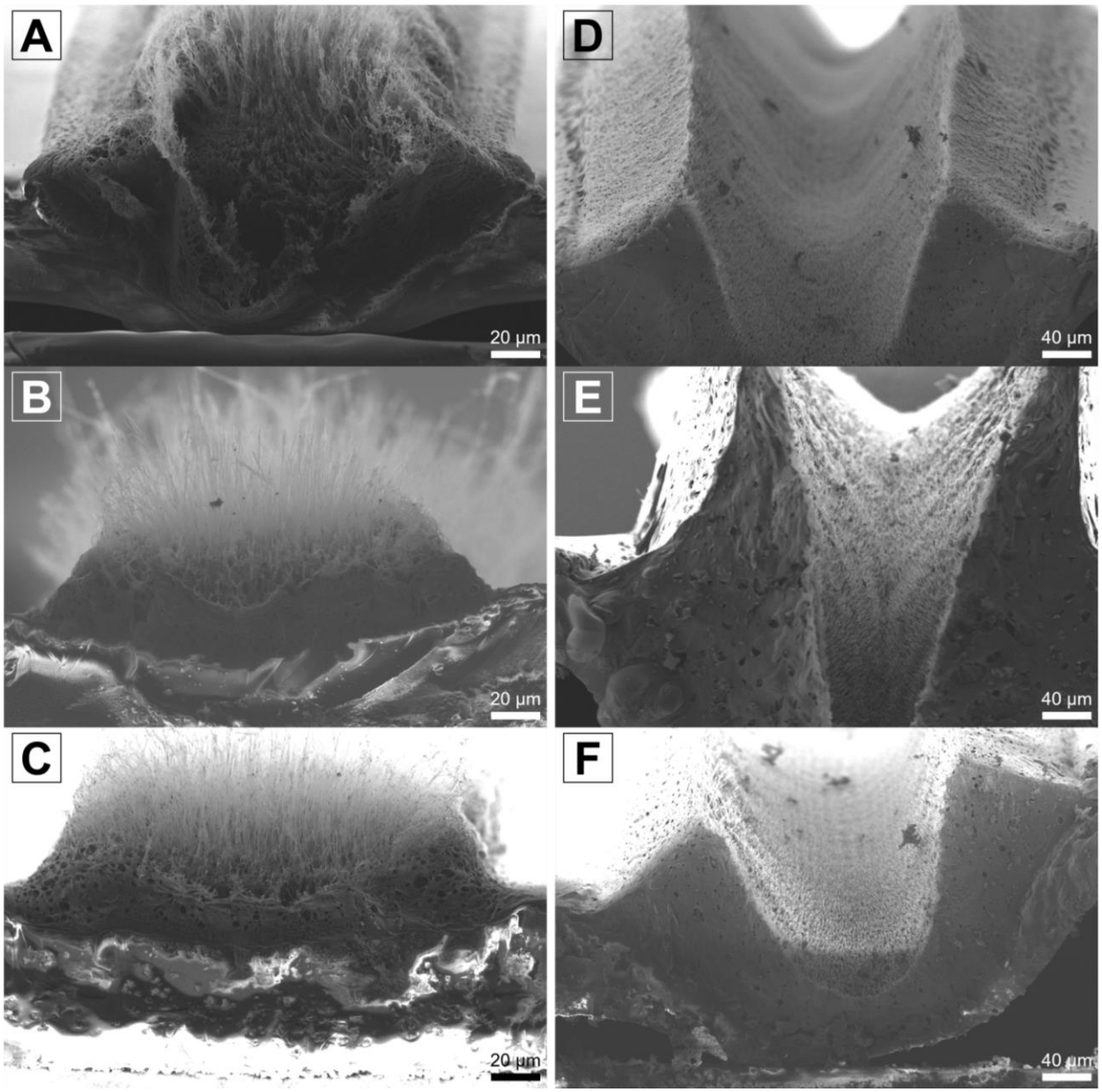

Fig. S2. Cross-sectional SEM images of carbon line features fabricated at P = 12.5 W, S = 500 mm s^{-1} (laser fluence = 16 J cm^{-2}): (a) N-LINC, (b) F-LINC, and (c) S-LINC. Cross-sectional SEM images of carbon line features fabricated at P = 12.5 W, S = 47 mm s^{-1} (laser fluence = 170 J cm^{-2}): (d) N-LINC, (e) F-LINC, and (f) S-LINC.

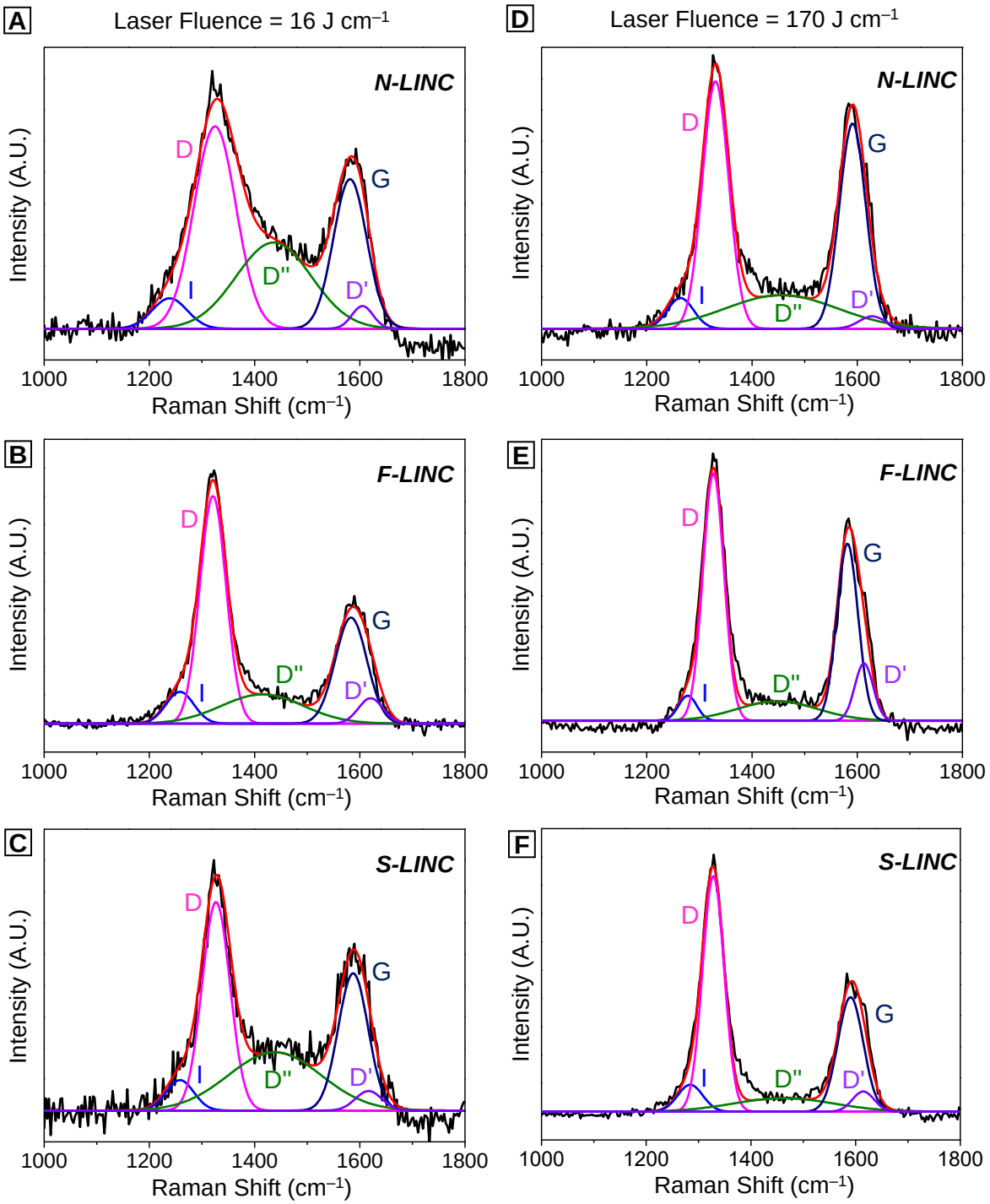

Fig. S3. Raman spectra and the deconvolution based on five Lorentzian peeks corresponding to the following bands bands: G, I, D, D', D''. Results obtained at laser fluence of 16 J cm^{-2} are presented for N-LINC in (A), F-LINC in (B), and S-LINC in (C). Results obtained at laser fluence of 170 J cm^{-2} are presented for N-LINC in (D), F-LINC in (E), and S-LINC in (F).

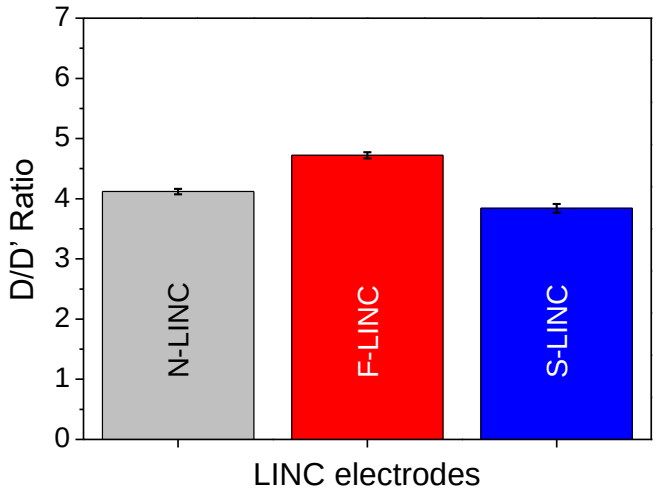

Fig. S4. The D/D' ratio of the three different LINC electrodes obtained at laser fluence of 170 J cm^{-2}.

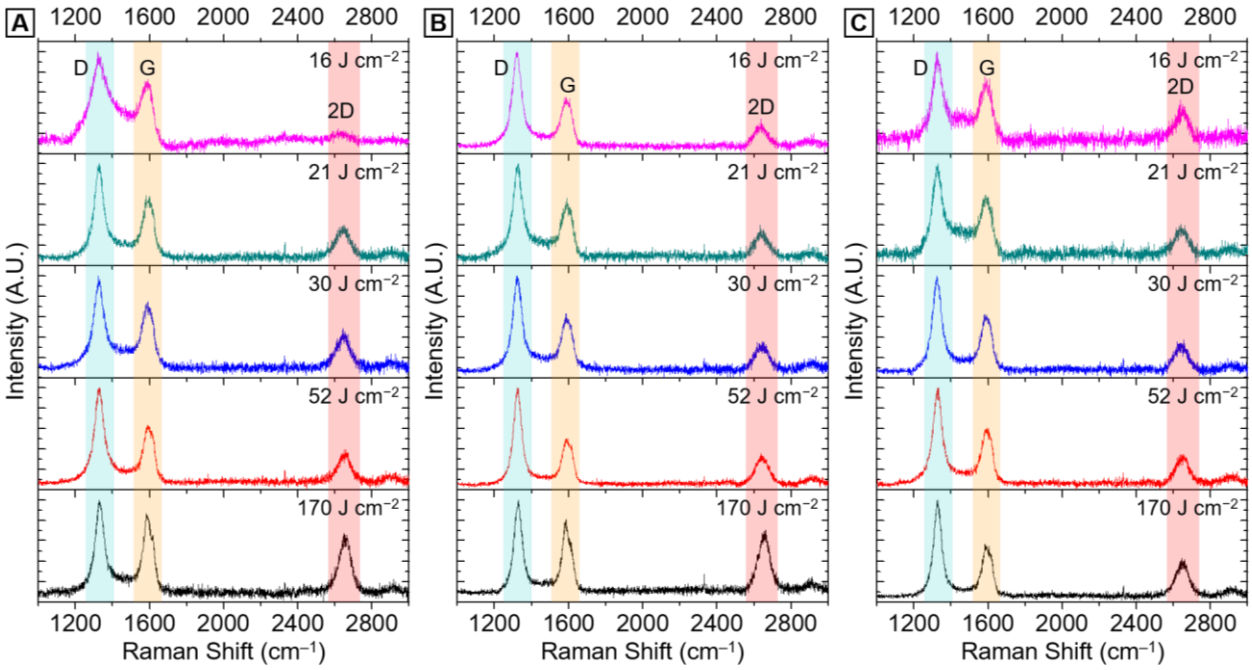

Fig. S5. Laser fluence dependent Raman spectra of carbon lines formed from (a) PMDA–ODA, (b) 6FDA–ODA, and (c) DSDA–ODA.

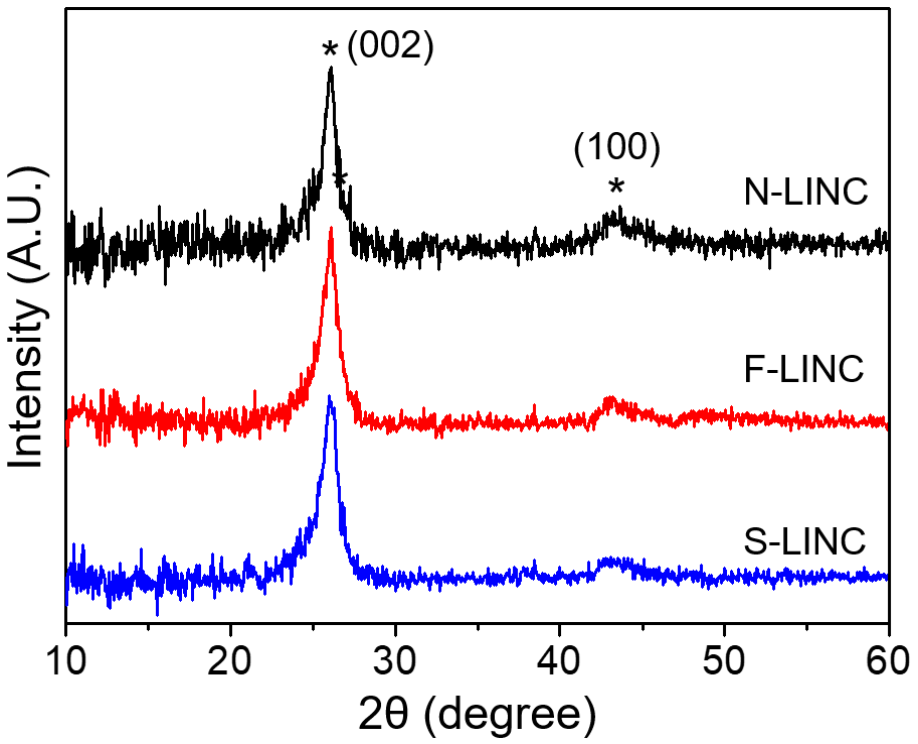

Fig. S6. XRD patterns of powdered N-LINC, F-LINC, and S-LINC scraped from the PI films. These samples were fabricated at fluence of 170 J.cm^{-2}.

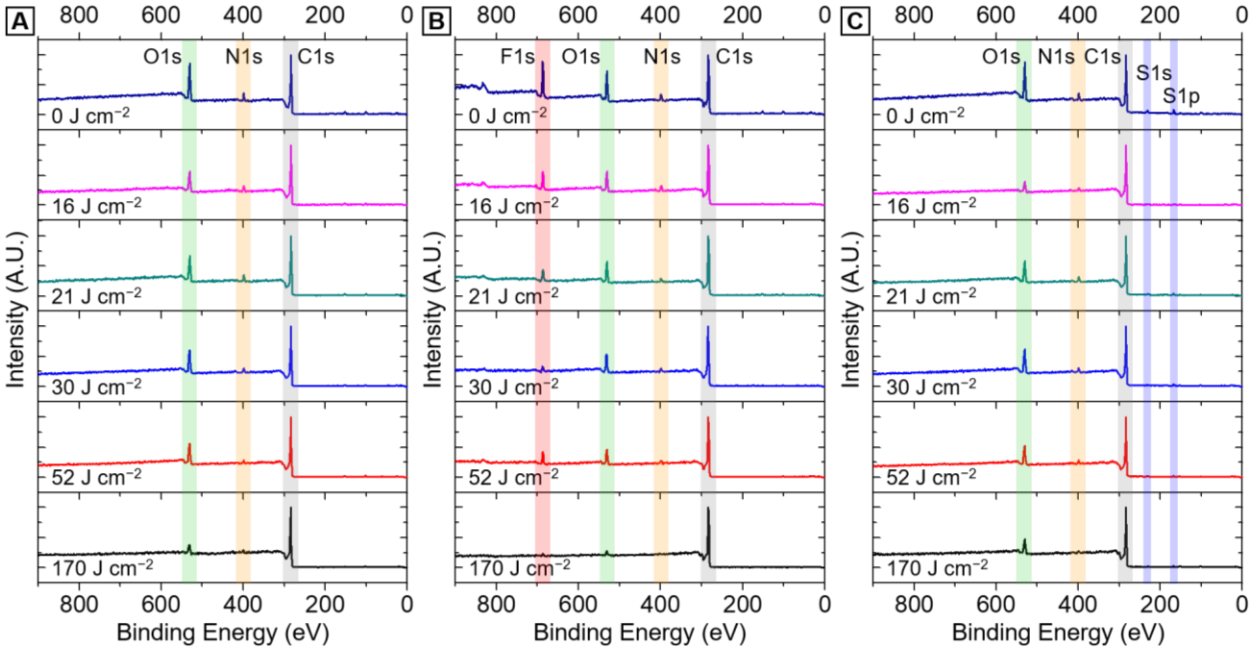

Fig. S7. Laser fluence dependent XPS survey spectra of carbon lines formed from (a) PMDA–ODA, (b) 6FDA–ODA, and (c) DSDA–ODA.

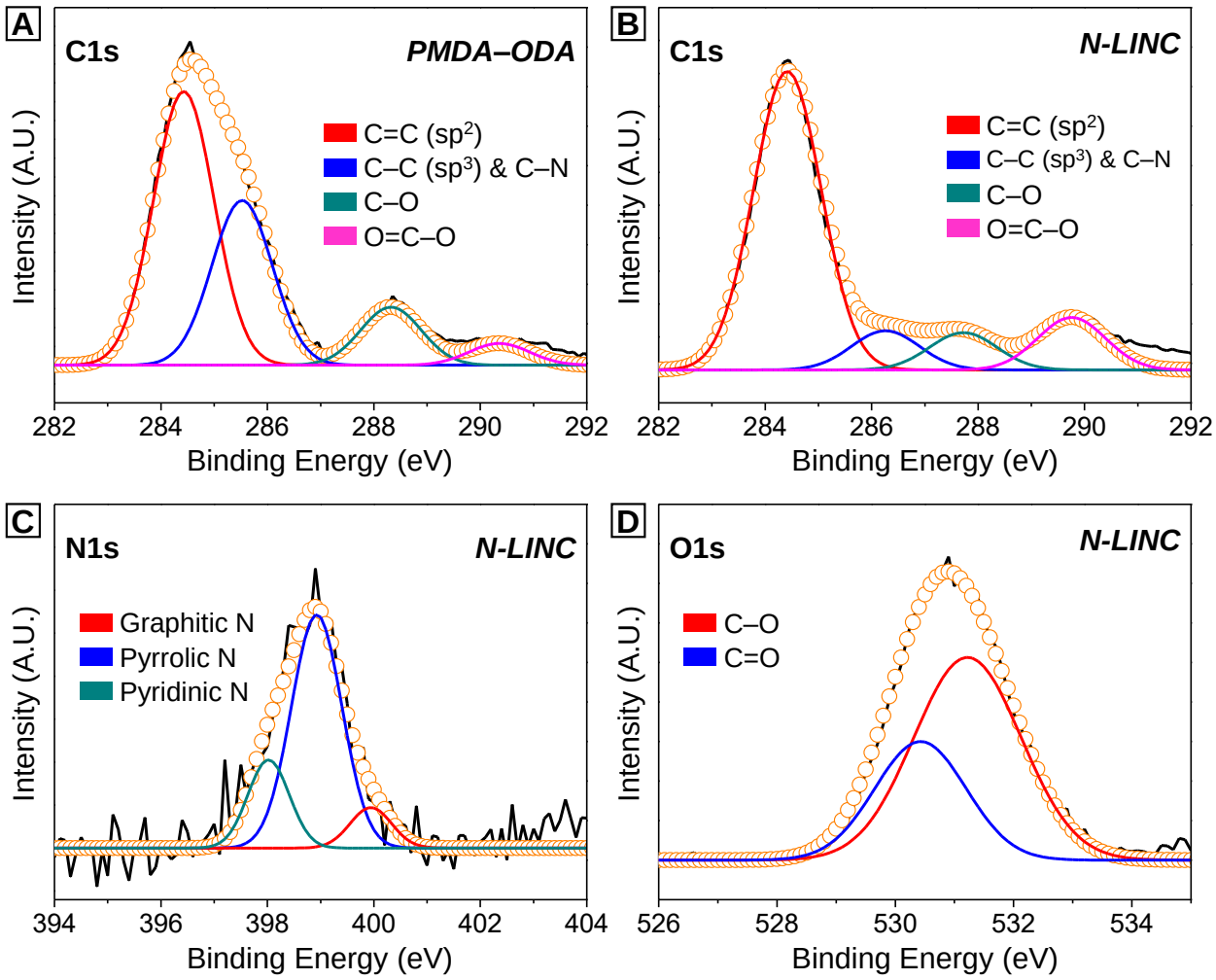

Fig. S8. N-LINC formed from PMDA–ODA at a laser fluence of 52 J cm^{-2} (P = 12.5 W, S = 153 mm s^{-1}). Deconvoluted (a–b) C1s XPS spectra of PMDA–ODA and N-LINC. High resolution (c) N1s and (d) O1s XPS spectra of N-LINC.

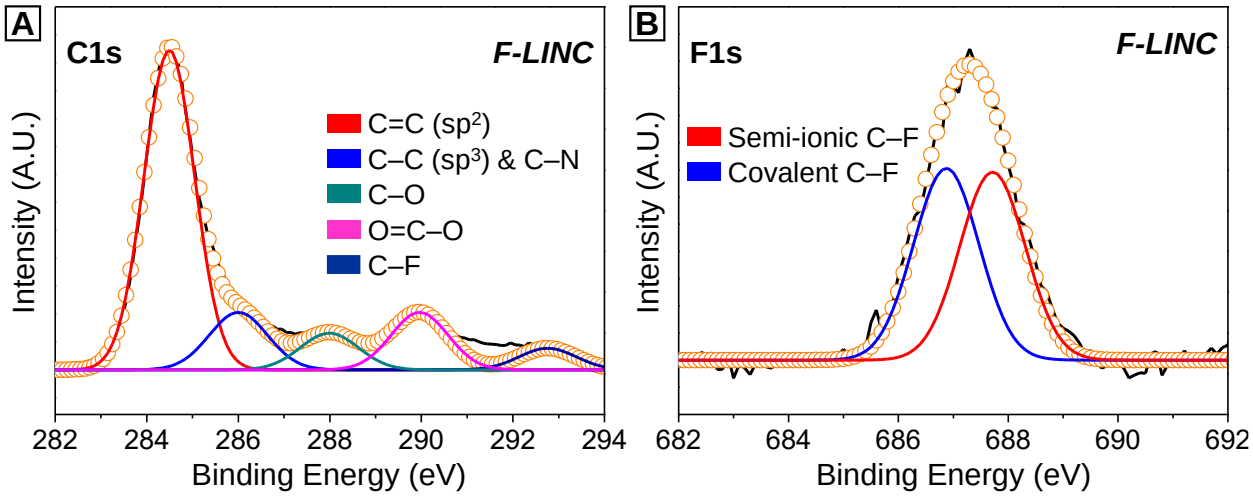

Fig. S9. F-LINC formed from 6FDA–ODA at a laser fluence of 52 J cm^{-2} (P = 12.5 W, S = 153 mm s^{-1}). Deconvoluted (a) C1s and (b) high resolution F1s XPS spectra of F-LINC.

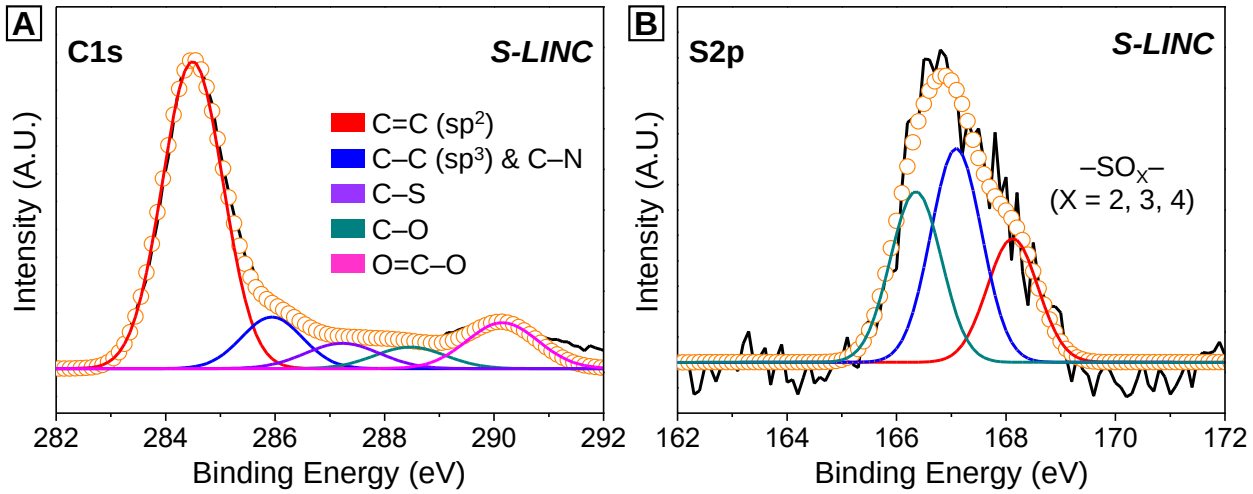

Fig. S10. S-LINC formed from DSDA–ODA at a laser fluence of 52 J cm^{-2} (P = 12.5 W, S = 153 mm s^{-1}). Deconvoluted (a) C1s and (b) high resolution S2p XPS spectra of S-LINC.

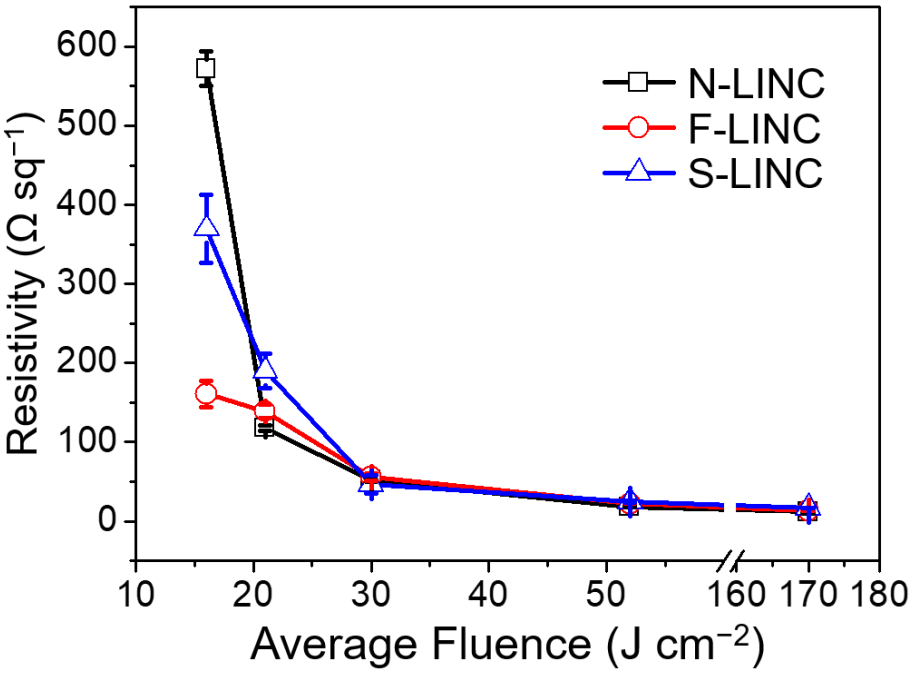

Fig. S11. Variation of resistivity of N-LINC (black line), F-LINC (red line), and S-LINC (blue line) with laser fluence.

Supplementary Notes

The beam is modeled as an elliptical Gaussian beam. The beam intensity is modeled using the following relationship.[4,5]

$$I(x,y,z) = I_o e^{-2\left(\frac{x}{w_x(z)}\right)^2} e^{-2\left(\frac{y}{w_y(z)}\right)^2} \left[\frac{W}{m^2}\right] \quad (1)$$

where x and y are measured from beam center axis at distance z from the beam waist. Beam dimensions are w_x and w_y based on $1/e^2$, and I_o is the maximum intensity.

Beam total power delivered at a spot with z vertical distance from the beam waist (estimated using thermopile measurements) is equal to the integration of the intensity over the laser spot in the horizontal plane (normal to the beam center axis), assuming complete absorption of the laser beam energy:

$$P = I_o \iint_{-\infty}^{\infty} e^{-2\left(\frac{x}{w_x}\right)^2} e^{-2\left(\frac{y}{w_y}\right)^2} dxdy \approx \frac{\pi}{2} I_o w_x w_y \quad (2)$$

where w_x and w_y are the $(1/e^2)$ beam size.

This integration approximately gives the value of the maximum intensity:

$$I_o(z) \approx \frac{2P}{\pi w_x(z) w_y(z)} \quad (3)$$

where P is constant for different z's, however the w_x and w_y change.

The Gaussian beam size at different z values is estimated using the following equations (assuming the beam spot major and minor axis is aligned with the lasing direction x and y):

$$w_x(z) = w_{ox}\sqrt{1 + \left(\frac{M_x^2 \lambda z}{\pi w_{ox}^2}\right)^2} \tag{4}$$

$$w_y(z) = w_{oy}\sqrt{1 + \left(\frac{M_y^2 \lambda z}{\pi w_{oy}^2}\right)^2} \tag{5}$$

where M_x^2 and M_y^2 are the beam quality factor for the x and y direction respectively, w_{ox} and w_{oy} are the beam waist dimensions. These parameters are estimated using the knife edge method as described in the supplementary information.

The average flux I_{av} is estimated at a certain spot size for a laser power P, by averaging the intensity $I(z)$ over the spot area $A(z)$:

$$\begin{aligned} I_{av}(z) &= \frac{\int_{-w_x(z)}^{w_x(z)} \int_{w_{y(z)}}^{w_y(z)} I(x,y,z)\,dy\,dx}{A(z)} \\ &= \frac{I_o}{\pi w_x(z) w_y(z)} \int_{-w_x(z)}^{w_x\,(z)} \int_{-w_y(z)}^{w_y(z)} e^{-2\left(\frac{x}{w_x(z)}\right)^2} e^{-2\left(\frac{y}{w_y(z)}\right)^2} dx\,dy \end{aligned} \tag{6}$$

The average fluence F is then estimated using the following relationship:

$$F(z,v) = D(z,v) I_{av}(z) \tag{7}$$

where D(z,v) is the dwell time of the laser beam over a spot. The dwell time is estimated by dividing the beam length in the lasing direction x by the beam speed v.[6]

$$D(z,v) = \frac{2w_x(z)}{v} \tag{8}$$

Supplementary Tables

Table S1. The experimental operating laser parameters of single paths at vertically fixed sample stage (Z-direction = distance of laser beam waist) and the corresponding accumulated fluences

Operating Laser Power (%)	Calculated Laser Power (W)	Operating Raster Speed (%)	Calculated Raster Speed (mm s^{-1})	Accumulated Laser Fluence (J cm^{-2})
30	12.5	1	47	170
		10	153	52
		20	218	37
		30	269	30
		40	312	26
		50	350	23
		60	384	21
		70	412	19
		80	445	18
		90	468	17
		100	500	16
40	18.3	100	500	23
50	23.2			30
60	28.1			36

Table S2. Summary of atomic percentage of the elements in pristine PI films and corresponding carbonized lines derived from different laser fluences

Sample Code	Laser Fluence (J cm^{-2})	Carbon (%)	Oxygen (%)	Nitrogen (%)	Fluorine (%)	Sulfur (%)
N-LINC	0	74.7	18.6	6.5	–	–
	16	82.3	11.2	6.3	–	–
	21	81.2	13.0	5.8	–	–
	30	83.4	12.8	3.9	–	–
	52	83.6	12.8	3.5	–	–
	170	88.5	7.6	3.9	–	–
F-LINC	0	67.8	13.6	5.4	13.1	–
	16	76.3	10.9	5.3	7.6	–
	21	78.0	11.4	5.3	5.2	–
	30	82.2	11.1	3.6	3.1	–
	52	83.2	9.1	2.2	5.5	–
	170	94.6	3.4	–	2.0	–
S-LINC	0	72.2	19.1	6.0	–	2.7
	16	81.4	12.0	5.0	–	1.6
	21	79.1	12.8	6.0	–	2.1
	30	81.3	13.6	3.7	–	1.4
	52	84.2	11.2	3.6	–	1.1
	170	89.5	9.6	–	–	1.0

Table S3. Summary of deconvolution of XPS C1s spectra in Figures S8−10

Sample Code	Deconvolved peak	Binding Energy (eV)
PMDA–ODA	C=C (sp^2)	284.5
	C–C (sp^3) & C–N	285.6
	C–O	288.3
	O=C–O	290.4
N-LINC*	C=C (sp^2)	284.5
	C–C (sp^3) & C–N	286.3
	C–O	287.8
	O=C–O	289.8
F-LINC*	C=C (sp^2)	284.5
	C–C (sp^3) & C–N	286.0
	C–O	288.0
	O=C–O	290.0
	C–F	292.7
S-LINC*	C=C (sp^2)	284.5
	C–C (sp^3) & C–N	285.9
	C–S	287.2
	C–O	288.4
	O=C–O	290.1

* Samples were lased at fluence of 52 J cm^{-2}

References

[1] K.H. Nam, H. Kim, H.K. Choi, H. Yeo, M. Goh, J. Yu, J.R. Hahn, H. Han, B.C. Ku, N.H. You, Thermomechanical and optical properties of molecularly controlled polyimides derived from ester derivatives, Polymer (Guildf). 108 (2017) 502–512. https://doi.org/10.1016/j.polymer.2016.11.062.

[2] H. Yeo, M. Goh, B.C. Ku, N.H. You, Synthesis and characterization of highly-fluorinated colorless polyimides derived from 4,4′-((perfluoro-[1,1′-biphenyl]-4,4′-diyl)bis(oxy))bis(2,6-dimethylaniline) and aromatic dianhydrides, Polymer (Guildf). 76 (2015) 280–286. https://doi.org/10.1016/j.polymer.2015.09.019.

[3] J.G. Liu, Y. Nakamura, Y. Shibasaki, S. Ando, M. Ueda, High refractive index polyimides derived from 2,7-bis(4- aminophenylenesulfanyl)thianthrene and aromatic dianhydrides, Macromolecules. 40 (2007) 4614–4620. https://doi.org/10.1021/ma070706e.

[4] R. Poprawe, K. Boucke, D. Hoffman, Tailored Light 1, 2018. https://doi.org/10.1007/978-3-642-01234-1.

[5] R. Poprawe, Tailored Light 2 Laser Applicaiton Technology, Springer, 2004.

[6] J. Jiang, A.G. Jacobs, B. Wenning, C. Liedel, M.O. Thompson, C.K. Ober, Ultrafast Self-Assembly of Sub-10 nm Block Copolymer Nanostructures by Solvent-Free High-Temperature Laser Annealing, ACS Appl. Mater. Interfaces. 9 (2017) 31317–31324. https://doi.org/10.1021/acsami.7b00774.